Chapter 5

Coexistence of Spin-Valve like magnetoresistance and anomalous Hall effect in $Ni_2MnSn_{1-x}Alx(x = 0.5)$

5.1 Introduction

Nickel-manganese $(Ni-Mn-X)$ based Heusler alloys, incorporating main group element (X= Si, Sn, Al, In, Ga and B) display remarkable physical properties stemming from the intricate interplay between their structural and magnetic characteristics [Agarwal et al. (2018); Guha et al. (2020); Krenke et al. (2005); Muthu et al. (2013); Patel et al. (2022); Singh et al. (2022)]. These alloys, whether adhering to stoichiometric ratios or deviating from them, are renowned for their diverse range of physical phenomena [(Dubenko et al. (2014)]. These phenomena encompass magnetic shape memory effects, magnetoelasticity, magnetic glass, asymmetric magnetoresistance, and various multifunctional attributes. An intriguing observation has been the manifestation of asymmetric resistance switching in response to modest magnetic fields, denoting a substantial low-field magnetoresistance (MR)[(Dieny et al. (1991)]. This phenomenon is generally attributed to disparities in

spin-dependent electron scattering, which arise from alterations in the orientation of adjacent magnetic layers concerning the applied magnetic field direction. It has been detected not only in artificial magnetic multilayer heterostructures like spin valves and magnetic tunnel junctions but also in magnetic multilayer structures based on Heusler alloys[(Hirohata et al. (2015); Nag et al. (2022); Singh et al. (2012); Venkateswara et al. (2023)]. Nevertheless, witnessing such a pronounced low-field asymmetric MR in bulk materials remains relatively rare. This peculiarity might be ascribed to the interference of macrostructural changes in the vicinity, hindering the aforementioned switching behaviour in bulk systems. Alternatively, a distinct mechanism may underlie the spin-valve-like MR observed in bulk Mn_2NiGa Heusler alloys[(Singh et al. (2012)]. This mechanism is elucidated as arising from the coupling of Mn atoms positioned in the Ga sites, giving rise to ferromagnetic nanoclusters that are antiferromagnetically coupled to other Mn atoms. The spin valve effect is the basis for many magnetic sensors and read heads in hard disk drives and other magnetic storage devices. It has also been fundamental in the development of spintronic devices, which utilize the spin of electrons, in addition to their charge, to process and store information more efficiently[Hirohata & Takanashi (2014)].

Furthermore, another captivating phenomenon commonly encountered in Heusler alloys is the Anomalous Hall effect (AHE). Currently, there is immense interest in the AHE due to its potential applications in spintronics such as for magnetic sensors and memory devices [(Chiba et al. (2010); Ohno et al. (2000)]. The Hall effect, a well-established phenomenon, signifies the generation of a transverse voltage in a current-carrying conductor when an external magnetic field is applied perpendicular to the current's direction. The AHE introduces an additional component in the transverse voltage, as witnessed in materials with broken time-reversal symmetry (TRS). This intriguing effect emerges due to the intricate interplay between magnetization and spin-orbit coupling (SOC). Despite being discovered over a century ago, the AHE has recently garnered substantial inter-

est owing to its role in elucidating fundamental physics and its potential applications in spintronics-based data storage devices and Hall sensors [Hirohata & Takanashi (2014)]. Theoretical investigations propose that the AHE may stem from both extrinsic and intrinsic mechanisms. Extrinsic contributions are linked to skew scattering and side jump mechanisms, which are associated with asymmetric scattering and transverse deviations in the paths of spin-polarized charge carriers[(Yue & Jin (2017)]. In contrast, the intrinsic mechanism is related to the momentum space Berry curvature connected to the electronic band structure. This Berry curvature effectively acts as a fictitious magnetic field, introducing an anomalous velocity perpendicular to the electric field direction. This, in turn, results in the intrinsic anomalous Hall conductivity (AHC) within the system[(Tian et al. (2009)]. Currently, researchers are deeply engrossed in investigating frustrated structures, noncollinear magnetism, as well as spin-ice and spin-liquid states, which have emerged as captivating subjects in the realm of Anomalous Hall Effect (AHE) research. In our present study, we align with the suggested "spin cluster" mechanism proposed by Ishizuka and Nagaosa[(Nagaosa et al. (2010)]. In this mechanism, when an external magnetic field induces a perturbation in the local order, magnetic fluctuations come into play as scattering centres. These fluctuations boost the skew scattering potential, which is a crucial aspect of our investigation. In the present work, a detailed study of the structural, magnetic, and transport properties of the NMSA system was done. The X-ray diffraction pattern suggests the presence of antisite disorder in the system. The magnetic study again shows the presence of mixed interaction due to the disordered state of the system. The system showed the SV-like behavior. The presence of AHE is observed up to room temperature, and extrinsic skew scattering is the dominating mechanism responsible for the AHE.

5.2 Experimental Details

The polycrystalline ingot of NMSA is prepared by the standard Arc melting process. For this, the constituents elements Ni, Mn, Sn, and Al with purity of 99.95% were taken in a stoichiometric ratio. The sample is melted several times to ensure the homogeneity. Then the melted ingot was sealed in a quartz tube under a base pressure of $10^{-}6$ mbar. This quartz tube is placed inside of the furnace at 1073 K for seven days for the annealing process then the quartz tube is quenched into the ice water after seven days. The prepared ingot was crushed into the fine powder to record the powder XRD of the sample. The powder XRD was done using the Rigaku MiniFlex II DESKTOP powder diffractometer ($CuK\alpha radiation, \lambda = 1.54184$). The Rietveld refinement of the X-ray spectra is done using the Fullprof software to determine the lattice parameter and atomic position of the system. A rectangular piece for transport properties is cut of dimensions 1.28 mm $\times$ 0.62 mm $\times$ 0.23 mm using the diamond cutter. The physical properties of the system are measured by the Physical Properties Measurement System (Quantum Design). For longitudinal resistivity, the ρ_{xx} four probe method is used for which the probe was made using the silver paste and gold wires. The current of magnitude 3 mA is applied in the X- direction and voltage is also measured in the X- direction. For magneto-transport, the current is applied along the X-direction, and magnetic field (B) is applied perpendicular to the sample, let's say Z-direction and voltage is measured along the X-direction. The transverse resistivity ρ_{xx} is measured in which the voltage is measured along Y-direction. The Magnetic measurements of the system were performed using a superconducting quantum interference device-based magnetometer (MPMS, Quantum Design. contacts were made on the thin strip of the sample using epoxy silver paste and platinum wires. The current of 1 mA was driven through the outer contacts using a current source and the voltage was measured using the inner contacts.

5.3 Results and Discussions

5.3.1 Structural Characterisation

To investigate the crystal structure of the $Ni_2MnAl_{0.5}Sn_{0.5}$ Heusler compound, powder X-ray diffraction (PXRD) patterns were collected at room temperature. Heusler alloys typically exhibit an L_21 crystal structure, with the space group F$\bar{4}$3m. The superstructure reflections (111) and (200) are also observed, implying the pattern is related to the regular L_21 phase. Therefore, initially, a Rietveld refinement was performed assuming the L_21 crystal structure figure 5.1b (a), utilizing the FULLPROF software package. In the refinement process, the Wyckoff positions were assigned as follows: the Mn atoms were located at the 4b position (1/2, 1/2, 1/2), denoted as Mn 4b, while the Ni atoms occupied the 8c position (3/4, 3/4, 3/4). Additionally, the Al and Sn atoms were found to share the 4a position at (0, 0, 0). The lattice parameter obtained after the refinement was 5.95 , reduced due to the presence of the Al atom, which has a smaller atomic radius than Sn (Datta et al. (2022)). Due to the comparable atomic radius of Mn and Sn, there can be partial occupancy exchanged in their respective positions. Hence chemically disordered state is expected, which has a great effect on physical parameters. The intensity of the (200) peak is small due to the negligible difference between the atomic structure factor of Ni and Mn (Webster (1969); Wittmann, Baker & § (Wittmann et al.)). The crystal structure with partial disorder between the Mn and Sn was simulated from the VESTA as shown figure 5.1b (b). In which Mn and Sn both sharing their positions indicated the presence of antisite disorder in the system. The XRD pattern of NMSA indicates that the system also contains a small amount of martensitic phase and it is denoted by M in figure 5.1b (a). This indicates that the system persists in a martensite phase at room temperature. This finding is also consistent with other Heusler systems having a martensite phase at room temperature Ahuja et al. (2010); Singh et al. (2010).

(a) (b)

Fig. 5.1 (a) Room temperature powder XRD of NMSA (b) unit cell drawing using VESTA software showing the antisite disorder

5.3.2 Isothermal Magnetization

The isothermal curve is recorded at an applied external field of 200 Oe in both zero-field cooled warming (ZFCW) and field-cooled warming (FCW) protocols as given in figure 5.2. The magnetization versus temperature (M(T)) curves were measured under Zero Field Cooling (ZFC) and Field-Cooled Warming (FCW) protocols, with a field strength of 200 Oe. Initially, the ZFC and FCW measurements exhibited similar behavior and retraced each other up to the temperature of 270 K. However, at this temperature, a bifurcation occurred between the ZFC and FCW curves, indicating the presence of mixed ferromagnetic and antiferromagnetic interactions in the system. In the temperature range from room temperature down to 270 K, the magnetization increased as the temperature decreased, suggesting a ferromagnetic behavior. The presence of two different crystal symmetries in the alloy, as confirmed by X-ray diffraction (XRD) analysis, contributes to this observation. However, below 250 K, a decrease in magnetization with temperature was observed in both the ZFC and FCW conditions. This decrease signifies the presence of an antiferromagnetic (AFM) phase in the system, which effectively lowers the overall magnetization. The M(T) curve measured at a higher external field of 500 Oe reveals interesting findings. Initially, as the temperature decreases, the magnetization of the system increases, indicating a ferromagnetic ordering behavior. However, after reaching a temperature of 250 K, a bifurcation

occurs in the M(T) curve. Notably, the bifurcation temperature observed at 500 Oe is lower compared to the measurement at 200 Oe, suggesting a field-dependent effect. The magnitude of the bifurcation in the M(T) curve is also reduced at 500 Oe. This implies that the application of a higher external magnetic field tends to suppress the bifurcation. It indicates that the system exhibits anisotropic behavior primarily under small applied magnetic fields.

To understand the magnetic interaction more deeply, the isothermal magnetization (M(H)) of the system is recorded at different temperatures. The M(H) curves recorded at 2 K, show a rapid increase in moment at low field regions while showing a saturation behavior above 500 Oe. Saturation at the moment suggests ferromagnetic ordering in low temperatures. When the M(H) curve is recorded at 260 K, a similar behaviour is observed as the previous one but with two different things first is moment is decreased in comparison to the low temperature and after a rapid increase in moment up to 300 Oe, it increases linearly not showing any saturation. This type of behaviour suggests the presence AFM phase in the system. Similar results are also found for 300 K. It shows a more non-saturate nature at high fields. All the MH curve shows the presence of mixed interaction in the system, which again is due to the presence of two phases in the system. The isothermal magnetization (M(H)) of the system was measured at different temperatures to gain a deeper understanding of the magnetic interaction. At a temperature of 2K, the M(H) curve exhibited a rapid increase in magnetic moment at low field regions, followed by saturation behavior above 500 Oe. The saturation of the moment at low temperatures indicates the presence of ferromagnetic ordering. At a temperature of 260 K, a similar behaviour was observed, with two notable differences. Firstly, the magnetic moment was reduced compared to the low-temperature measurement. Secondly, after a rapid increase in the moment up to 300 Oe, the moment exhibited a linear increase without reaching saturation. This behaviour suggests the presence of an antiferromagnetic (AFM) phase in the system.

Similar results are also observed at 300 K, with a more pronounced non-saturating nature at high fields. The presence of mixed interaction in all M(H) curves indicates the coexistence of two phases within the system. The anisotropy in the system is due to the fact that the system possessed an antiside disorder in it. Due to this in the case of the regular L_21 structure Mn atom shares the ferromagnetic interaction between them while due to the partial occupancy of Mn at Sn site offers an antiferromagnetic interaction between the Mn atom and it is clear from the magnetic data also that as we increase the temperature the antiferromagnetic ordering dominates and it reduces the magnetization of the system and offered high resistance to the electrons therefore resistivity increases with decreasing temperature. hence system possesses an inbuilt anisotropy in it. Sometimes the system showing anisotropy is a potential candidate for the applications like exchange bias effect and spin valve-like effect.

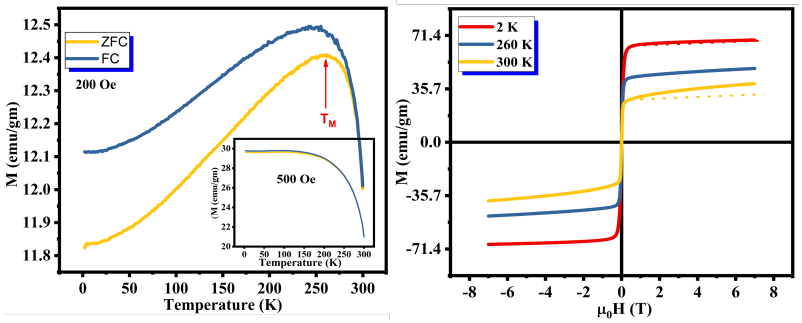

Fig. 5.2 Temperature dependent magnetization (M(T)) at 200 Oe in ZFC and FC protocols, Inset showing the (M(T)) curve for 500 Oe field. (b) Isothermal magnetization at 2 K, 260 K, and 300 K.

5.3.3 Transport Properties

The longitudinal resistivity ρ_{xx} was measured using four probe method (shown in figure 5.4) in the temperature range of 2 to 300 K, shown in figure 5.3. Initially, ρ_{xx} is decreased upto 240K with increasing temperature and after 240 K it increased further and showed metallic nature. The ρ_{xx} of the martensitic phase differs notably from that of the austenitic phase,

exhibiting a higher resistance than in comparison to the austenite phase. This disparity in resistivity occurs during this transition, and changes in magnetic scattering patterns occur, resulting in enhanced electron scattering from various orientations of martensitic variants within the material. Further ρ_{xx} showed an increase with temperature above MT; again, that was due to its structural changes. As in the austenite phase, the system is in the ordered state therefore, it would provide less scattering, and hence ρ_{xx} increases after 240 K. The change in resistivity with temperature is analogues to the temperature-dependent magnetization behaviour of the system. The change in resistivity is associated with enhanced magnetic scattering. This means that the scattering of electrons due to magnetic ions within the material plays a role in the observed increase in resistivity. As the resistivity increases, the magnetism of the alloy weakens in the vicinity of the martensitic transformation, as shown in figure 5.2 (a). Further, the residual resistivity ratio for the system defined as $(RRR = \rho_{300K}/\rho_{300K})$, which quantifies the degree of disorder, is obtained to be around 0.51, suggesting that the presence of disorder in the system. This is also confirmed from XRD data which proves the presence of antisite disordered state in the system. This implies a correlation between electrical and magnetic properties in the material.

The field-dependent longitudinal resistance was measured using the standard four-probe technique, as depicted in figure 5.4. Contacts were established on the thin rectangular sample using gold wires. A current of 3 mA was passed through the outer contacts using a current source, while the voltage was measured using the inner contacts. The current flowed along the x-direction, and the magnetic field was aligned along the z-axis. The magnetoresistance (MR) is defined as $\rho_{(H)} = \frac{\rho_H - \rho_0}{\rho_0}$, where ρ_H is the resistivity under a magnetic field H, and ρ_0 denotes the resistivity at zero magnetic field. The MR curves were captured at various temperatures ranging from 300 to 2 K, as illustrated in figure 5.5(a). Generally, the field-dependent MR is symmetric in nature in the applied external magnetic field. Interestingly, in NMSA, we noticed an asymmetric behaviour in MR while switching

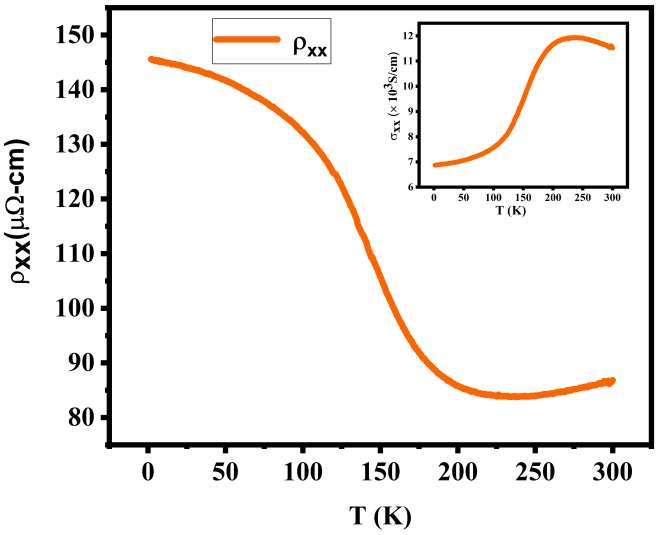

Fig. 5.3 Temperature-dependent longitudinal resistivity (ρ_{xx})

from negative to the positive field in the low field region from 2K to 300K as shown in the inset of figure 5.5 (b,d). Here the presence of asymmetric (MR_{ASYM}) was due to the structural transition which resembles the nature of spiv valve (SV) also. This behaviour is in close resemblance with the asymmetry in MR observed in other Heusler alloys like Mn_2NiGa and other quaternary Heusler Alloys [(Nag et al. (2022); Singh et al. (2012); Venkateswara et al. (2023)]. To separate out the (MR_{ASYM}) part, we have calculated the MR_{ASYM} which is defined as $MR_{ASYM} = (MR_{(H)} - MR_{(-H)})/2$, In MR_{ASYM}, the saturation is started from the field of 1.2 T. Generally, the asymmetry in MR is the consequence of the difference in scattering at the interfaces of the FM/AFM. In the present system, we have observed a magneto structural change which offered a change in scattering due to field-induced change in phase. Further, the symmetric part of the MR is calculated as $MR_{SYM} = MR_{(+H)} + MR_{(-H)})/2$; is negative and shows the linear variation with the field shown in figure 5.5(a). The negative MR (NMR) was due to the fact that as we increase the temperature its resistivity decreases hence, we have NMR. The MR_{SYM} is linear in nature is governed by the s-d scattering interaction, where s conduction electrons are scattered

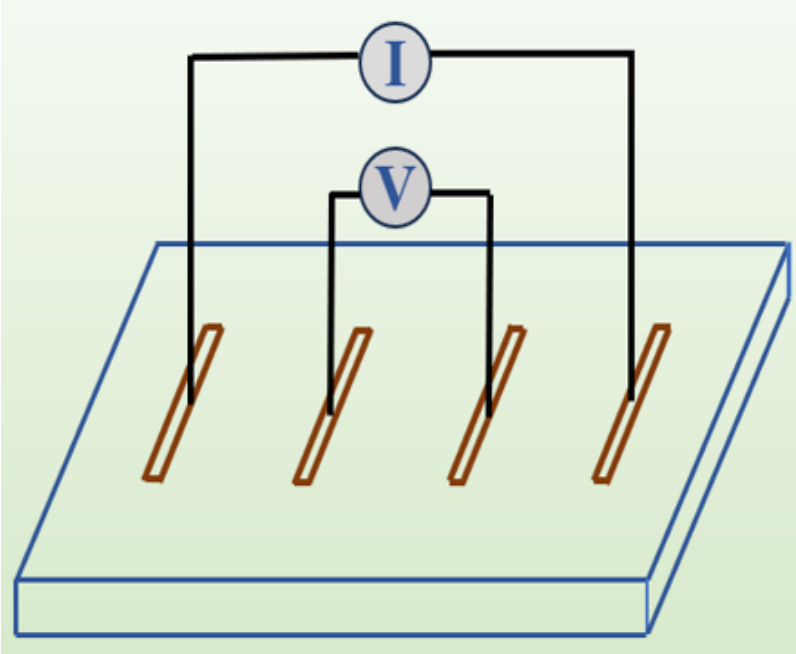

Fig. 5.4 Schematic representation of four probe setup

by localized d spins on the magnetic ions. We observed a relatively high value of MR at 300 K. The resistivity from 240 K onwards increases with increasing temperature, this is the reason behind the relatively high value of MR at 300 K. Furthermore, a cusp is also observed in the symmetric part of the MR at low field region. This cusp-like behaviour is diminished at temperature 300 K. so the observance of cusp in low field region was due to the shape memory effect of the system. In the martensite phase cusp like behaviour is observed in MR curve while as the system enters into the austenite phase this cusp is diminished [(Biswas et al. (2005)]. The observed behaviour of MR, which typically occurs in thin film heterostructures featuring two ferromagnetic layers separated by a nonmagnetic conducting layer, is also found in bulk Mn_2NiGa alloy Singh et al. (2010).

This phenomenon may be attributed to a slight disorder between Ga and Mn atoms, resulting in the formation of ferromagnetic nanoclusters within the Mn_2IrGa lattice. These clusters consist of parallel Mn spins within an antiparallel Mn spin matrix (Patel et al. (2023)). When a magnetic field is applied, the direction of Mn moments in the soft

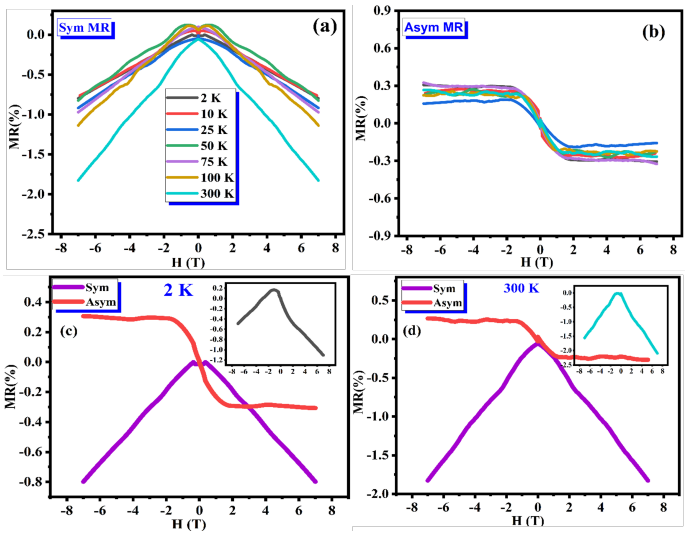

Fig. 5.5 (a) Symmetric part of the MR (b) Asymmetric nature of MR (c) and (d) showing the both components of MR at 2K and 300 K inset showing the TOTAL MR (SYM+ASYM)

ferromagnetic clusters' reverses, causing a rotation or tilt in the antiparallel Mn moments at the interface between the clusters and the lattice. As a consequence, an asymmetry in the magnetoresistance is observed. Here in this system as it is clear from the XRD data that system exhibited an antisite disorder, which means that some atoms of Mn shared the position with Al/Sn atoms. It is clear from the literature for Ni- based alloys, when Mn is sharing its position with non-magnetic elements like Sn or Al then the antiferromagnetic interactions are dominating between the Mn-Mn. In case of pure L_21 structure ferromagnetic ordering is dominant. So, for this system, antisite disorder as well as the magneto structural change is responsible for the presence of SV like MR in the system. The asymmetric part of the MR resembles like the M-H curve of the system, it also saturates at small fields like magnetization curve.

5.4 Hall effect

After thoroughly examining the phase purity, magnetic properties and magnetoresistance of the system we proceeded to study the magneto transport study of the system. Firstly, the

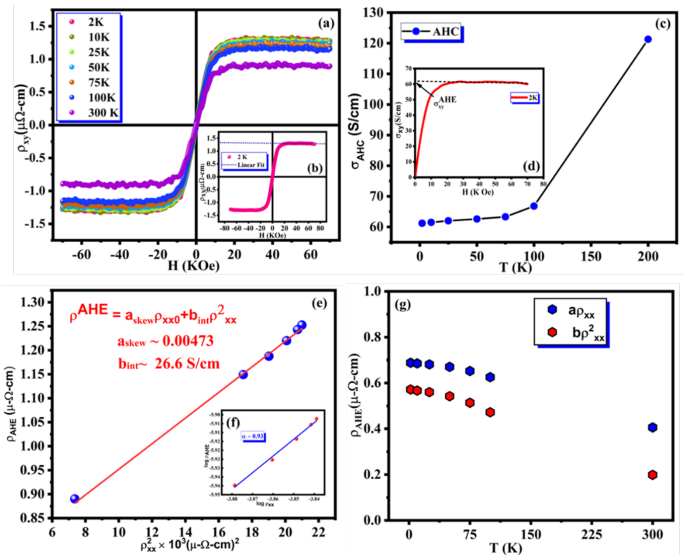

Fig. 5.6 (a) Field-dependent Hall resistivity curves at different temperatures. (b) inset shows the linear fit of xy at 2 K (c) Field-dependent Hall conductivity curve at various temperatures (d) inset shows the zero-field extrapolation of high-field Hall conductivity data at 2 K; (e) variation in anomalous Hall conductivity with temperature; (f) linear fit of the ρ_{xy} vs. ρ^2_{xx} curve. Inset shows the linear fit on the logarithmic scale between ρ_{xy} vs. ρ_{xx} logarithmic scale between (h) shows the separate contribution coming from both mechanisms.

presence of structural change in the system. As it is clear from the M (T) curve the system possesses a structural change around 260 K, which is a transition from paramagnetic austenite to the martensite phase. Since NMSA exhibits magneto structural transitions. Therefore, it is useful to study the AHE to explore the understanding of the mechanism involved in the AHE. The Hall resistivity (ρ_{xy}) measurement was done for the system in the temperature range of 2K to 300 K as shown in figure 5.6 (a). The Hall resistivity shows a steep increase in the low field regions (up to 15 KOe) while at higher field regions it shows a linear behaviour. This steep increase in the low field region indicates the presence of Anomalous Hall effect (AHE). We know that due to the magnetic nature of the system an extra term is added to the hall resistivity, which can be defined as;

$$\rho_{xy} = R_0 H + R_s M_s \tag{5.1}$$

Here, R_o,R_s is the ordinary, anomalous Hall coefficient respectively and M_s is the magnetisation of the system. The additional term R_s M_s which is called as AHE is due to the magnetization of the system. As the magnetization of the system gets saturated after 1 tesla field hence it is independent of the external magnetic field hence this contribution is only due to the intrinsic magnetic nature of the system. To extract the anomalous hall contribution from the total Hall, The Hall resistivity was fitted linearly in the high field region as shown in the inset of figure 5.6 (a). The slope and intercept after linear fit provide the value of R_o and R_s M_s respectively. Tine et al. established some scaling relations [Tian et al. (2009)], in order to find the mechanism involved in the AHE. As from the experiment data it was impossible to separate the mechanism involved in the origin of AHE so it is better to use scaling relation to separate out the possibility of every term responsible for the AHE. The mechanism responsible for the AHE can be checked by the dependency relation between $\rho_{xy} \propto \rho_{xx}^{\alpha}$. If α =1 then the contribution is coming solely from the extrinsic skew scattering and for α = 2 the combination of intrinsic and side jump is responsible for the presence of AHE. To separate the contributions of both mechanisms, an equation is defined that extracts the contributions of both terms.

$$\rho_{xy}^{AHE} = a\rho_{xx0} + b\rho_{xx}^{2} \tag{5.2}$$

Here ‘a’ is the contribution due to the extrinsic skew scattering and b showed the contribution from the both intrinsic and side jump scattering. After using the above equation, the value of a and b comes out 0.0042 and 27 S/cm. The change in anomalous Hall conductivity σ_{AHC} with temperature and/or longitudinal conductivity σ_{xx} also holds the information about the mechanism involved in the AHE. For this, the σ_{xy} was extracted by using the following relation,

$$\sigma_{xy} = \frac{\rho_{xy}}{\rho_{xy}^2 + \rho_{xx}^2} \tag{5.3}$$

Figure 5.6 (c) shows the σ_{xy} at different temperatures. For the value of AHC, zero field extrapolation of the high field σ_{xy} is done as shown in the inset of figure 5.6 (c). We have found that The value of AHC is 60 S/cm at 2 K. This is approximately two times larger than what we have observed from the several times smaller than then what we have observed after fitting the above equation. This indicates that the AHE in the present system arises due to both intrinsic as well as extrinsic skew scattering mechanisms. Figure 5.6 (g) shows that extrinsic skew scattering $(a\rho_{xx0})$ is dominated in the AHE than the intrinsic $(b\rho_{xx}^2)$ mechanism.

5.5 Conclusion

Here, we report a system $Ni_2MnSn_{0.5}Al_{0.5}$ which holds potential properties like Spin Valve and Anomalous Hall effect upto room temperature. The presence of spin valve is confirmed by the magnetization of the system. The M(T) curves of the alloy demonstrate a complex behaviour, with indications of both ferromagnetic and antiferromagnetic interactions. The occurrence of a bifurcation between the ZFC and FCW curves at 270 K suggests the presence of a mixed state in the system. Furthermore, the presence of antiside disorder in the system is revealed by XRD analysis, contributes to the observed magnetization behaviour. In summary, the M(T) curve measured at 500 Oe confirms a ferromagnetic ordering in the system, as indicated by the initial increase in magnetization with decreasing temperature. The occurrence of a lower bifurcation temperature and its suppression under higher external fields suggest the presence of field-dependent effects and anisotropic behaviour in the system, particularly noticeable under small applied magnetic fields. The resistivity of a material changes during a phase transition from austenitic to martensitic,

emphasizing the role of electronic band structure, magneto-structural transition, magnetic scattering, and the orientation of martensitic variants in this process. The observed changes in resistivity are indicative of alterations in the material's electrical and magnetic properties. Furthermore, We have carried out a detailed analysis of AHE NMSA, in which the scaling relation between ρ_{xy} and ρ_{xx} is $\rho_{xy} \propto \rho_{xx}^{\alpha}$. The almost linear dependence $(\alpha = 1)$ suggests that AHE originates from an extrinsic skew scattering mechanism. Therefore, the scaling law confirms that the dominating mechanism in AHE is extrinsic skew scattering. While the obtained value of intrinsic AHC (27 S/cm) is two times smaller than the obtained experimental value (60 S/cm at 2K). This again confirms that extrinsic contribution is the dominating mechanism for the AHE in NMSA system. In conclusion, the coexistence of many interesting properties in a single material opens up new opportunities for numerous applications such as magnetic sensors, and shape memory effect.